AMERICAN JOURNAL OF PHYSIOLOGY
HEART AND CIRCULATORY PHYSIOLOGY

Am J Physiol Heart Circ Physiol 330: H1935–H1950, 2026.
First published May 1, 2026; doi:10.1152/ajpheart.00540.2025

RESEARCH ARTICLE

Integrative Cardiovascular Physiology and Pathophysiology

Do small-conductance Ca^{2+}-activated K^+-channels contribute to ventricular repolarization in human heart failure?

Aiman Saleh A. Mohammed,[1]* Vivien Demeter-Haludka,[1,2]* Alaa Amin E. Abdelmagid,[1] Leila Topal,[1] Naveed Muhammad,[1] Gábor Mohácsi,[1] Benjamin Paskuj,[1] Gergő Bitay,[1] Zsófia Kohajda,[2] Kálmán Benke,[3] Alex Ali Sayour,[3] Tamás Radovits,[3] Miklós Bitay,[4] László Virág,[1] Norbert Jost,[1,2,5] István Baczkó,[1,5] András Varró,[1,2,5] Béla Merkely,[3]* and Norbert Nagy[1,2,5]*

[1]*Department of Pharmacology and Pharmacotherapy, Faculty of Medicine, University of Szeged, Szeged, Hungary;* [2]*HUN-REN-SZTE Research Group for Cardiovascular Pharmacology, Szeged, Hungary;* [3]*Heart and Vascular Center, Semmelweis University, Budapest, Hungary;* [4]*Division of Cardiac Surgery, Department of Internal Medicine and Cardiology Center, University of Szeged, Szeged, Hungary; and* [5]*Pharmaceutical and Medical Device Developments Competence Centre, Life Sciences Cluster, Centre of Excellence for Interdisciplinary Research, Development and Innovation, University of Szeged, Szeged, Hungary*

Abstract

Chronic heart failure constitutes a clinical syndrome characterized by substantial attenuation of repolarization reserve resulting from electrical remodeling. The small-conductance Ca^{2+}-activated K^+ channel (SK) has been reported to undergo upregulation in animal heart failure models and in human preparations; however, its exact function is not fully understood. This study aims to elucidate the functional role of SK channels in end-stage human heart failure. SK-protein expression of undiseased and failed human ventricular tissue was investigated by Western blot technique. Action potentials were measured by the standard microelectrode technique from right ventricular papillary muscles of undiseased hearts and from right and left papillary muscles and from left midmyocardial tissue slices of failing hearts. Ionic currents were recorded by the whole cell configuration of the patch-clamp technique on isolated cells obtained from left ventricles of failing hearts. Failing hearts exerted consistent action potential lengthening and lacked spike-and-dome compared with undiseased hearts. Western blot revealed identical SK expression between undiseased and failing hearts. Apamin (100 nM), a commonly used selective SK channel inhibitor, failed to alter action potential duration values of the failing hearts in left and right endocardial preparations and in left midmyocardium. Furthermore, no apamin-sensitive current was identified in isolated cells. Week coupling between SK2 channels and L-type Ca^{2+} channels was found. These results do not confirm the results of previous studies claiming an important role of SK channels in the repolarization of the human failing heart.

NEW & NOTEWORTHY This study re-evaluates the role of small-conductance Ca^{2+}-activated K^+ (SK) channels in ventricular repolarization in terminal human heart failure. Although SK protein is present and pharmacological activation causes only minor AP shortening, apamin does not affect action potentials or membrane currents, even with enhanced intracellular Ca^{2+}. Partial I_{Kr} block alone induces repolarization failure, indicating severely reduced repolarization reserve and negligible compensatory SK current, questioning the therapeutic relevance of SK channels in end-stage heart failure.

action potential; apamin; arrhythmia; heart failure; SK-channel

INTRODUCTION

Small-conductance Ca^{2+}-activated K^+-channels are encoded by KCNN1, -2, and -3 genes and expressed in both atrial and in ventricular tissue (1). Although these channels were discovered in the heart more than 30 years ago, the function of SK channels is still not fully elucidated. In 2003, Xu et al. (1) claimed that SK channels play a crucial role in ventricular and atrial repolarization in both humans and rats. However, this claim has been debated in both earlier and more recent studies (2, 3). Recently, it is generally accepted that SK-channels have no role in ventricular repolarization under normal condition (4–7), but their potential importance was suggested in heart failure (5, 6, 8, 9).

*A. S. A. Mohammed and V. Demeter-Haludka contributed equally to this work. B. Merkely and N. Nagy contributed equally to this work.
Correspondence: N. Nagy (nagy.norbert@med.u-szeged.hu).
Submitted 17 July 2025 / Revised 4 August 2025 / Accepted 27 April 2026

Table 1. *Heart failure patients*

No.	Gender	Age	BW, kg	BMI	Etiology	NYHA	BPSys, Hgmm	BPDia, Hgmm	HR, beat/min	EF, %	Drugs
1.	Male	47	87	24.9	DCM	IV.	80	60	NaN	16	RAM, CARV, WAR, ROS
2.	Male	57	101	29.5	DM	III.	58	79	75	28	BIS, EPL, WAR, SAC/VAL, FUR
3.	Male	53	98	32.7	DCM	III.	110	67	53	39	CARV, EPL, SAC/VAL, IVA, FUR, ATR, ALL
4.	Female	59	60	19.6	DCM	II.	107	55	73	22	BIS, SPR, SAC/VAL, FUR, AMIO
5.	Male	60	79	27.2	IHD	III.	100	70	60	18	RAM, FUR
6.	Male	54	86	27	DCM	III.	69	47	81	23	BIS, SPR, SAC/VAL, FUR, WAR, ROS
7.	Male	45	110	31.8	IHD	III.	110	70	72	15	RAM, CARV, AML, EPL, WAR, ASA, ATR
8.	Male	52	91	31.5	DCM	II.	103	59	55	19	MET, SPR, SAC/VAL, FUR, AMIO, WAR, ATR, ALL
9.	Male	24	58	19.2	HCM	II.	123	64	55	65	MET, KCl
10.	Male	60	93	25	DCM	III.	105	72	71	17	BIS, EPL, FUR, CLO, ALL, LEV, DAP, ZOL
11.	Male	45	53	17.3	IHD	IV.	112	89	71	25	EPL, FUR, ENOX, CLO, DOB, LEV, CLIN, DAP
12.	Female	38	90	33.1	DCM	III.	95	59	89	28	BIS, SPR, SAC/VAL, FUR, API, ATR, DAP, PAN
13.	Female	46	72	24.9	DCM	IV.	80	60	81	13	BIS, SPR, SAC/VAL, FUR, JAR
Mean		49 ± 2	83 ± 5	26 ± 2			98 ± 5	64 ± 3	70 ± 4	25 ± 2	

BPDia, diastolic blood pressure; BPSys: systolic blood pressure; BW, body weight; EF, ejection fraction; HR, heart rate. Drug treatment: ALL, Allopurinol; AMIO, Amiodaron; AML, Amlodipine; API, Apixaban; ASA, acetyl-salicilic acid; ATR, Atorvastatin; BIS, Bisoprolol; CARV, Carvedilol; CLIN, Clindamycine; CLO, Clopidogrel; DAP, Dapagliflosine; DOB, Dobutamine; EPL, Eplerenon; ENOX, Enoxaparine; FUR, Furosemide; IVA, Ivabradine; JAR, Jardiance, LEV, Levosimendan; MET, Metoprolol; PAN, Pantoprasole; RAM, Ramipril; ROS, Rosuvastatin; SAC/VAL, Sacubitril-Valsartan; SPR, Spironolacton; WAR, Warfarin; ZOL, Zolpidem.

Heart failure is characterized by profound electrical and structural remodeling, including attenuation of repolarization reserve, altered Ca^{2+} handling, and increased arrhythmia susceptibility (10). Several studies have reported upregulation of SK2 channels in cardiac hypertrophy and heart failure, in both experimental models and human tissue (8, 9, 11). This upregulation has been associated with increased Ca^{2+} sensitivity and altered channel regulation (8, 11–13). However, the functional consequences of enhanced SK channel expression remain debated. Depending on experimental conditions and

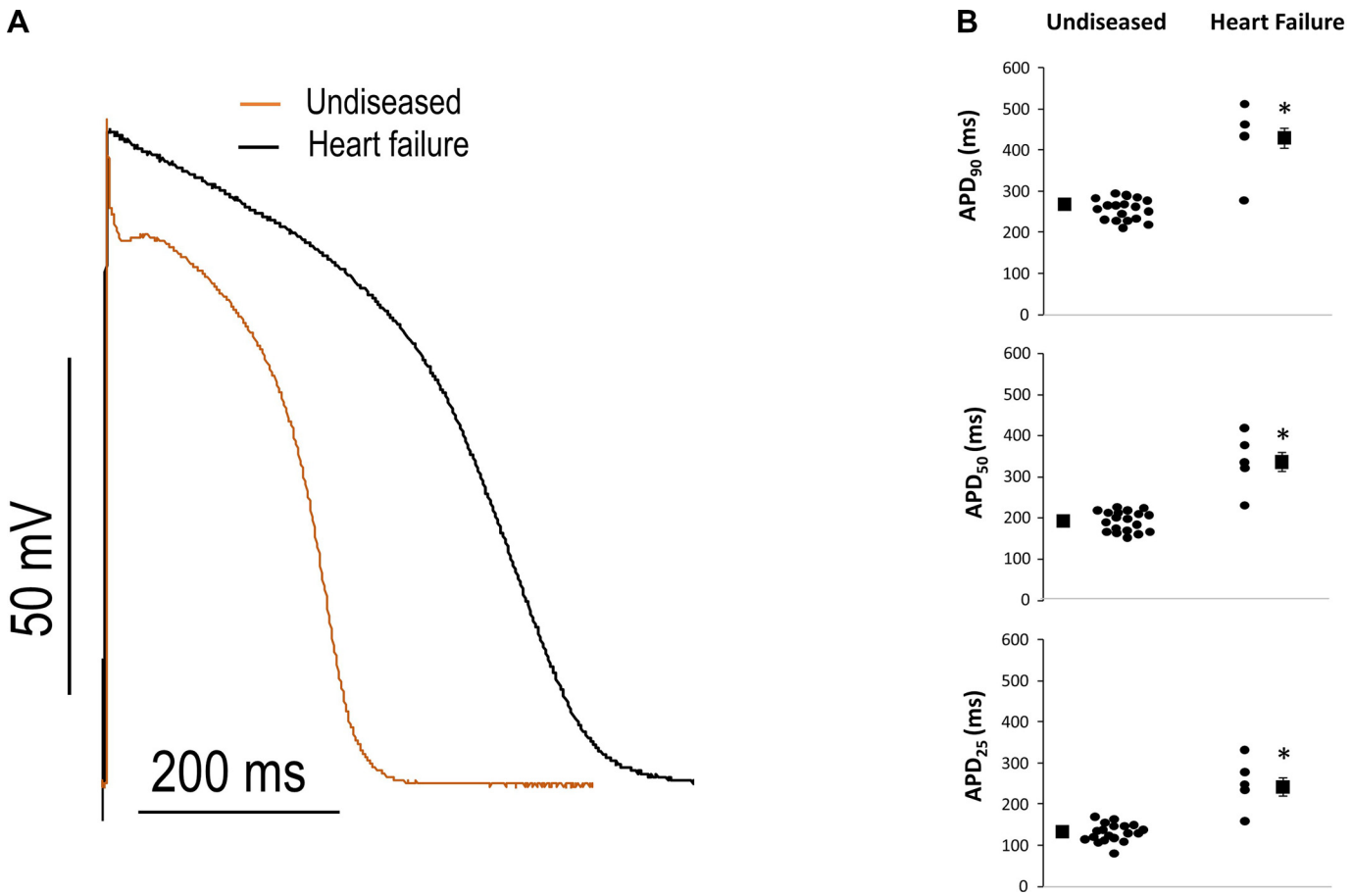

Figure 1. Comparison of human undiseased (brown trace) and failed (black trace) right ventricular action potentials. *A*: absence of notch, elevated plateau potentials and longer action potential duration (APD) was obvious in all preparations. *B*: values and means of APD_{90} (*top*), APD_{50} (*middle*), and APD_{25} (*bottom*) between undiseased (*left*) and failed (*right*) human heart. *N* = 19-5 patients respectively. *APD values were significantly larger in failing hearts.

disease models, SK channel activity has been described as either protective—by supporting repolarization reserve—or arrhythmogenic due to increased spatial heterogeneity of repolarization (5–7, 14).

In general, Ca^{2+}-dependent regulation of cardiac repolarization could have critical importance in several aspects (10). Thus, despite evidence for altered SK channel expression in heart failure, their actual electrophysiological contribution to ventricular repolarization in human failing myocardium remains unclear. Because SK channels directly couple intracellular Ca^{2+} dynamics to membrane potential, clarifying their functional role has particular importance in the context of heart failure-associated Ca^{2+} dysregulation and remodeling. Therefore, in the present paper we studied the possible role of SK current in end-stage failing hearts with reduced ejection fraction.

METHODS

Undiseased Donor Hearts

The investigations conformed to the principles of the Declaration of Helsinki. Human left ventricular (LV) biopsies were received for research purposes under approval from the Scientific and Research Ethical Committee of the Medical Scientific Board at the Hungarian Ministry of Health (ETT-TUKEB), Hungary, Number 4991-0/2010-1018EKU [339/PI/010]. Nonfailing myocardium was obtained from general organ donors whose hearts were not used for transplantation due to nonmedical reasons. Samples from nonfailing organ donors were procured under national presumed consent legislation in accordance with ETT-TUKEB regulations. Before cardiac explantation, the donors did not receive medication except furosemide, dobutamine, and plasma expanders.

Explanted Failing Hearts

The investigations conformed to the principles of the Declaration of Helsinki. In this study, 13 failing hearts were used, obtained after heart transplantation from the Semmelweis University Heart and Vascular Center, Budapest, Hungary. The mean age of the patients was 49 ± 2 yr. Ten male and three female hearts were included into the study (Table 1). After removal of the heart, left and right ventricular trabecules and right ventricular papillary muscles,

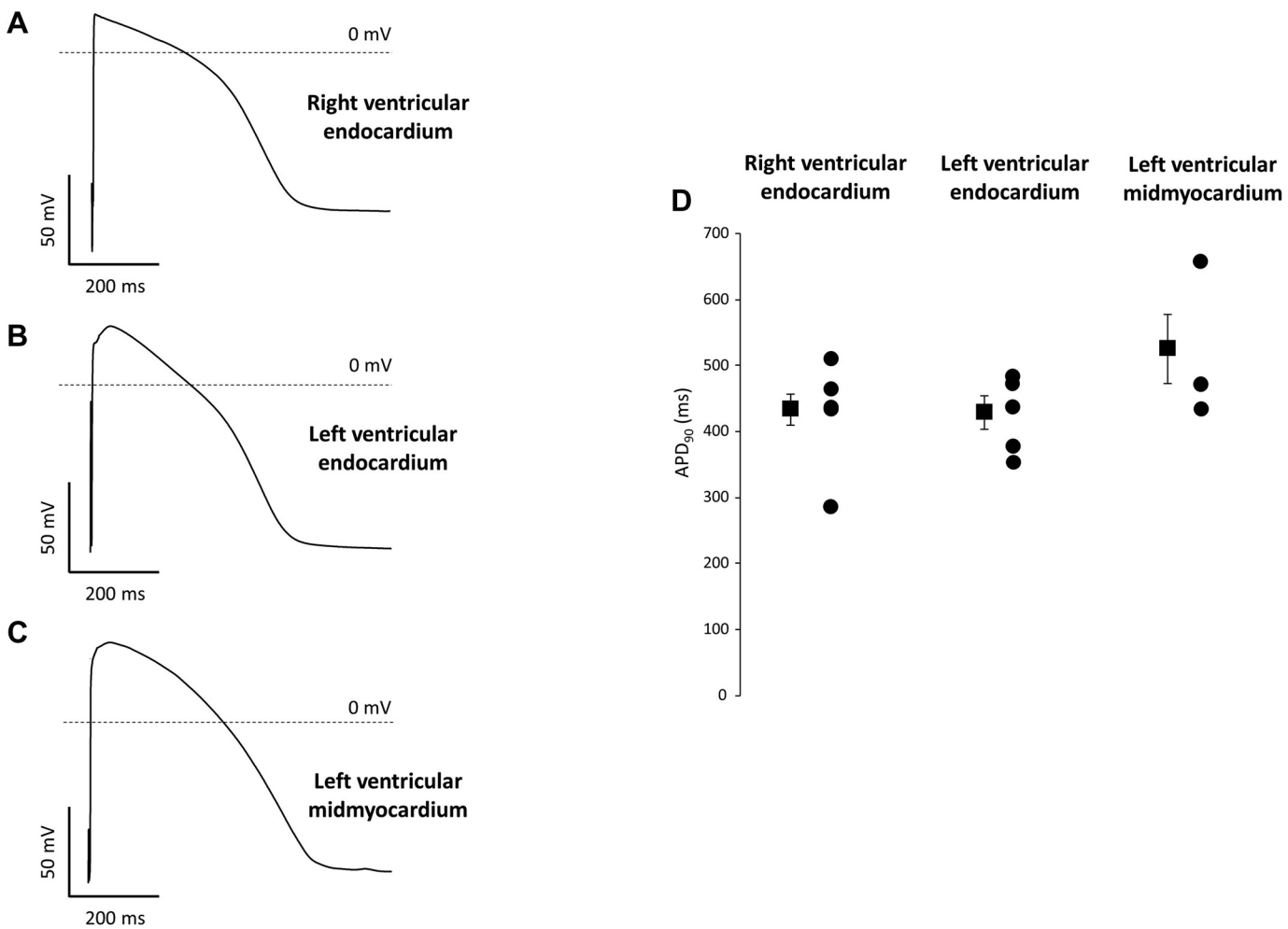

Figure 2. Comparison of different ventricular tissue layers obtained from failed human ventricle. Representative action potential traces obtained from right (*A*) and left (*B*) ventricular endocardium and left ventricular midmyocardium (*C*) were compared. *D*: individual action potential duration (APD_{90}) values (circle) as well as mean APD_{90} values (■) of action potentials. *N* = 5-5-3 patients respectively. No significant difference was observed.

left ventricular tissue segment for cell isolation, and left ventricular tissue cube for slicing were prepared, placed in Ringer-Lactate solution and transferred to the University of Szeged (Permit Number: IV-1185-1/2022/EKU). Written informed consent was obtained from all the heart failure patients whose cardiac tissue samples were involved in the study.

Preparations of Midmyocardial Tissue Slices

Approximately 1 cm side length tissue cube from the left ventricle and the epicardial surface was glued to the platform of the tissue chamber of vibratome (Vibratome 300 Sectioning System, Ted Pella Inc, CA) by using histoacryl tissue glue (Braun, Melsungen, Germany). Tissue chamber was filled with modified Locke's solution (in mM: 130 NaCl, 21.5 $NaHCO_3$, 4.5 KCl, 12 glucose, 0.4 $MgCl_2$, 1.8 $CaCl_2$, 10 2,3-butanedione-monoxime, pH 7.35 ± 0.05. Tissue slices (400-μm thickness) were cut by vibratome having progression speed of 0.05 mm/s and lateral blade vibration amplitude of 2 mm. Slices were recovered for 2 h then replaced to normal Locke's solution (i.e., without 2,3-butanedione-monoxime) for further 2 h during continuous carbogen bubbling.

Determination of the Action Potential Parameters in Multicellular Preparations

Action potentials (APs) were recorded at 37°C from the surface of right and left ventricular papillary muscles, trabecules, and from left ventricular tissue slice obtained from the midmyocardial layer using the conventional microelectrode technique. For measuring tissue APs, a similar protocol was applied as described earlier with minor modifications (11, 12). Briefly, the preparations were mounted in a custom-made Plexiglas chamber, allowing continuous superfusion with Locke's solution (130 mM NaCl, 21.5 mM $NaHCO_3$, 4.5 mM KCl, 12 mM glucose, 0.4 mM $MgCl_2$, 1.8 mM $CaCl_2$, pH 7.35 ± 0.05) and stimulated with constant pulses of 5-ms duration at a rate of 1 Hz through a pair of bipolar platinum electrodes using an electro-stimulator (EX-ST-A2, Experimetria Ltd.). Sharp microelectrodes with tip resistance of 10–20 MΩ, when filled with 3 M KCl, were connected to an amplifier (Biologic Amplifier, Model VF 102). Voltage output from the amplifier was sampled using an AD converter (NI 6025, Unisip Ltd.). APs were monitored and evaluated by using Evokewave v.1.49 (Unisip Ltd.).

Conventional S1S2 restitution protocol.

Extra test action potentials were elicited by using single test pulses (S2) after every 10th basic beat (S1) in a preparation driven at a basic cycle length (S1-S1) of 1,000 ms. The S1–S2 coupling interval was increased progressively from the end of the refractory period. The diastolic intervals preceding the test action potential were measured from the point corresponding to 90% of repolarization of the preceding basic beat to the upstroke of the test action potential and were increased progressively to 1,000 ms.

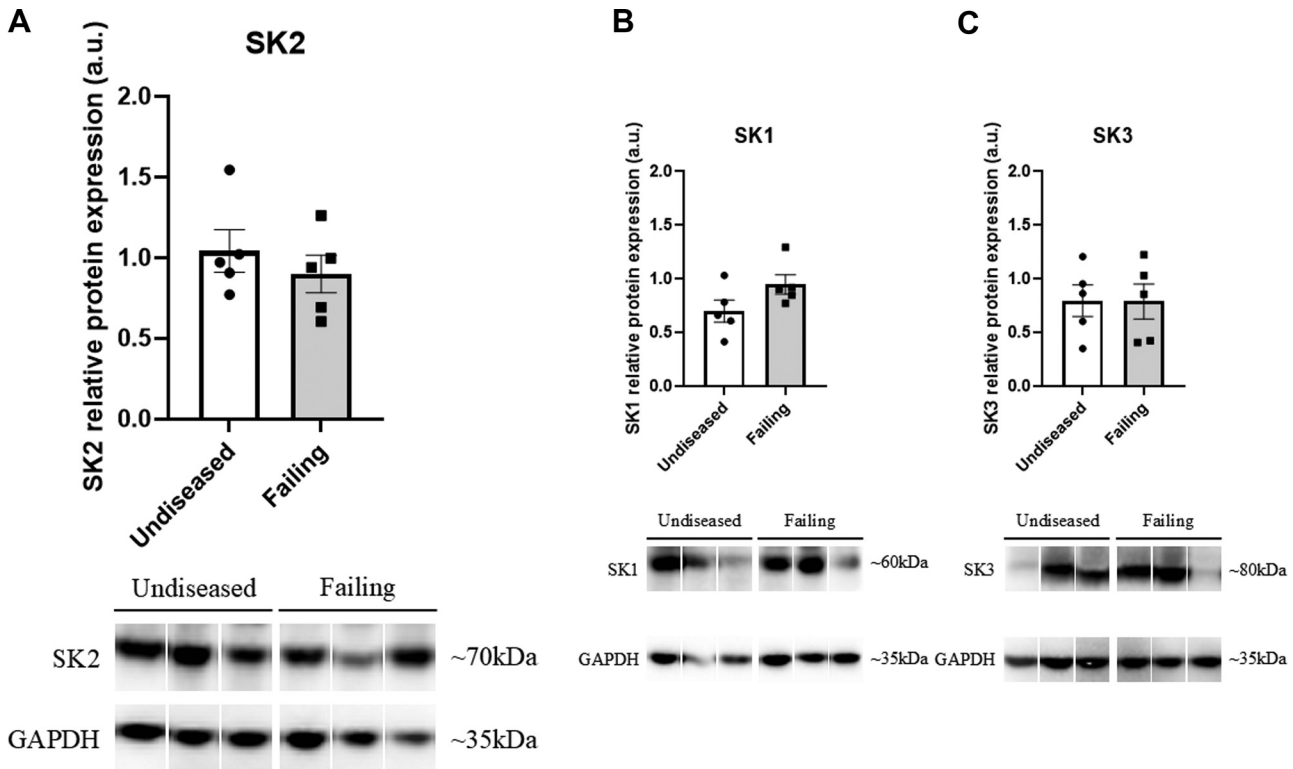

Figure 3. Small-conductance Ca^{2+}-activated K^+ (SK)1, SK2, and SK3 protein expression in the left ventricles of undiseased and failing hearts. Protein expression was assessed using a Western blot. The scatter plots in the *top* display the relative levels of SK1, SK2, or SK3, whereas the *bottom* show representative bands with their corresponding loading controls. *A*–*C*: membrane SK protein abundance did not differ significantly between undiseased and failing human hearts. For each patient, two bands were evaluated and averaged. Data are presented as means ± SE. $P < 0.05$ compared with undiseased hearts.

Cycle-length dependent protocol.
The pacing cycle length was gradually shortened to 400 ms from 1,000 ms then it was lengthened again up to 5,000 ms. Ten action potentials were recorded at each pacing cycle length.

Determination of SK1, SK2, and SK3 Protein Expression

SK1, SK2, and SK3 protein expression was assessed using Western blot analysis. Myocardial samples from the left ventricle were obtained from both undiseased and failing hearts ($N = 5$ in both groups). The membrane fraction was isolated as previously described (13). Protein concentrations were determined using the Bradford assay, and 20 μg of protein per sample was loaded onto 10% acrylamide gels for SDS-PAGE and then transferred onto PVDF membranes. After blocking the membranes with 5% nonfat dry milk for 1 h at room temperature, the membranes were probed overnight at 4°C with the primary antibodies, anti-SK1 (1:200, Alomone Labs, Cat. No. APC-039), anti-SK2 (1:200, Alomone Labs, Cat. No. APC-028), and anti-SK3 (1:200, Alomone Labs, Cat. No. APC-025). Following this, the membranes were incubated for 1 h at room temperature with the secondary antibody, horseradish peroxidase (HRP)-conjugated goat anti-rabbit IgG (1:8,000, Southern Biotech, 4030-05). Chemiluminescent signals were detected using the ECL Prime Western Blotting Detection Reagent (GE Healthcare) and visualized with the ChemiDoc Imaging System (Bio-Rad). GAPDH (1:10,000, Thermo Fisher Scientific, PA1-988) served as a loading control. Band intensities were quantified using ImageJ (FIJI) software (v.1.54p). To assess primary antibody specificity, membranes were incubated overnight with either the primary antibody alone or in the presence of the corresponding blocking peptide (1:100). Incubation with blocking peptides (SK1: Cat. No. BLP-PC039, SK2: Cat. No. BLP-PC028, SK3: Cat. No. BLP-PC025; Alomone Labs) served as negative controls. Blocking peptide controls are shown in Supplemental Fig. S1. For each patient, two bands from two separate Western blots were analyzed and averaged. The resulting data from individual patients in each group were then further averaged.

Assessment of SK2 and Cav1.2 Colocalization

SK2 and Cav1.2 colocalization was determined using multiple immunofluorescence labeling. Left ventricular tissue from failing human hearts ($N = 4$) was embedded in optimal cutting temperature (OCT) compound and cryosectioned. Sections (20 μm) were fixed with ice-cold acetone, rehydrated in PBS, and blocked with 2.5% BSA in PBS containing 0.1% Tween-20 for 1 h at room temperature. Sections were then probed overnight at 4°C with primary antibodies against SK2 (1:37.5, Alomone Labs, Cat. No. APC-028-GP, host: guinea pig) and Cav1.2 (1:37.5, Alomone Labs, Cat. No. ACC-003, host: rabbit). Following primary antibody incubation, sections were treated with Alexa Fluor 488-conjugated and Alexa Fluor 635-conjugated secondary antibodies (1:300; Thermo Fisher Scientific, Cat. No. A-11073 and A-31577) for 1 h at room temperature. Plasma membranes were labeled with Wheat Germ Agglutinin Texas Red-X conjugate (1:500, Thermo Fisher Scientific, Cat. No. W21405) for 30 min. Images were

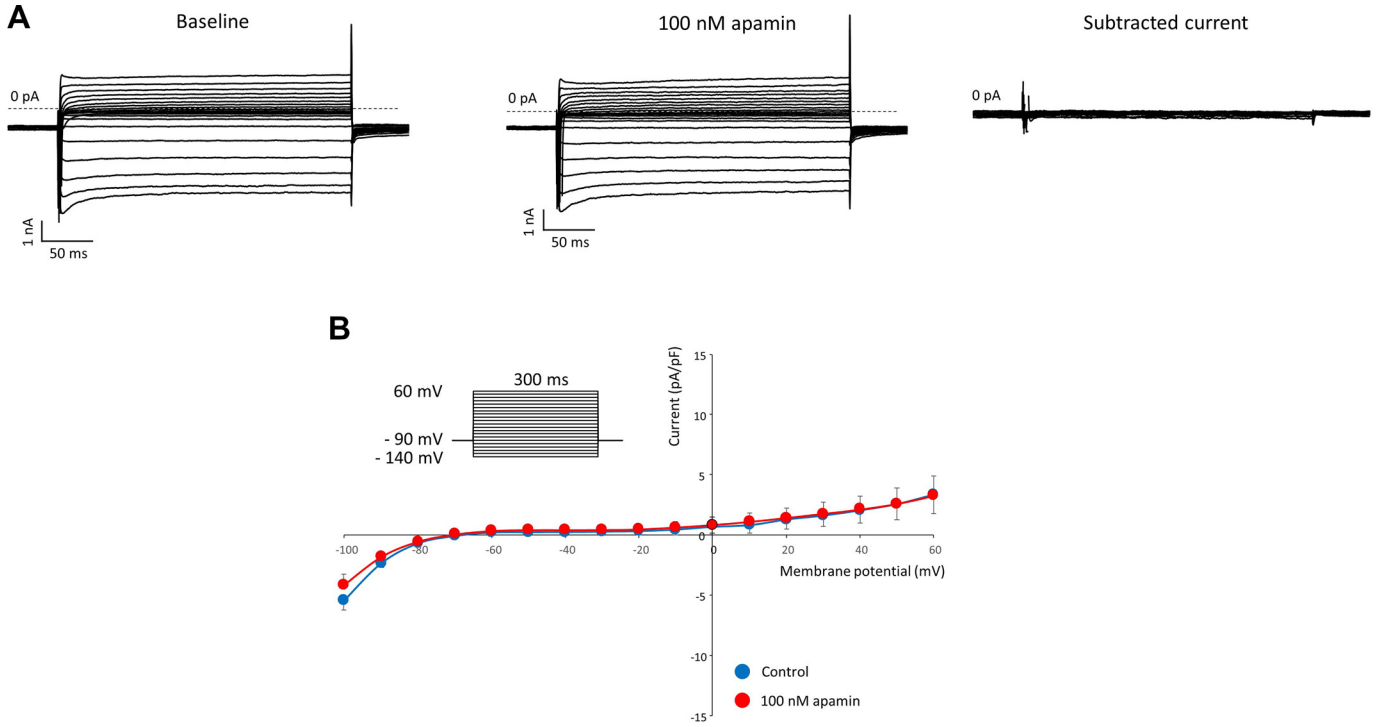

Figure 4. Measurement of apamin-sensitive current. *A*: representative current traces under control condition (*left*), after 100 nM apamin (*middle*), and current obtained after subtraction of apamin-treated traces from control (*right*). *B*: current-voltage relationship of the measured current under control condition (blue) and after 100 nM apamin. *Inset*: the applied voltage protocol. Note that the error bars are smaller than the symbols at some membrane potentials, and the measurements were performed down to −140 mV, the current is shown only up to −100 mV. $N = 4$ patients.

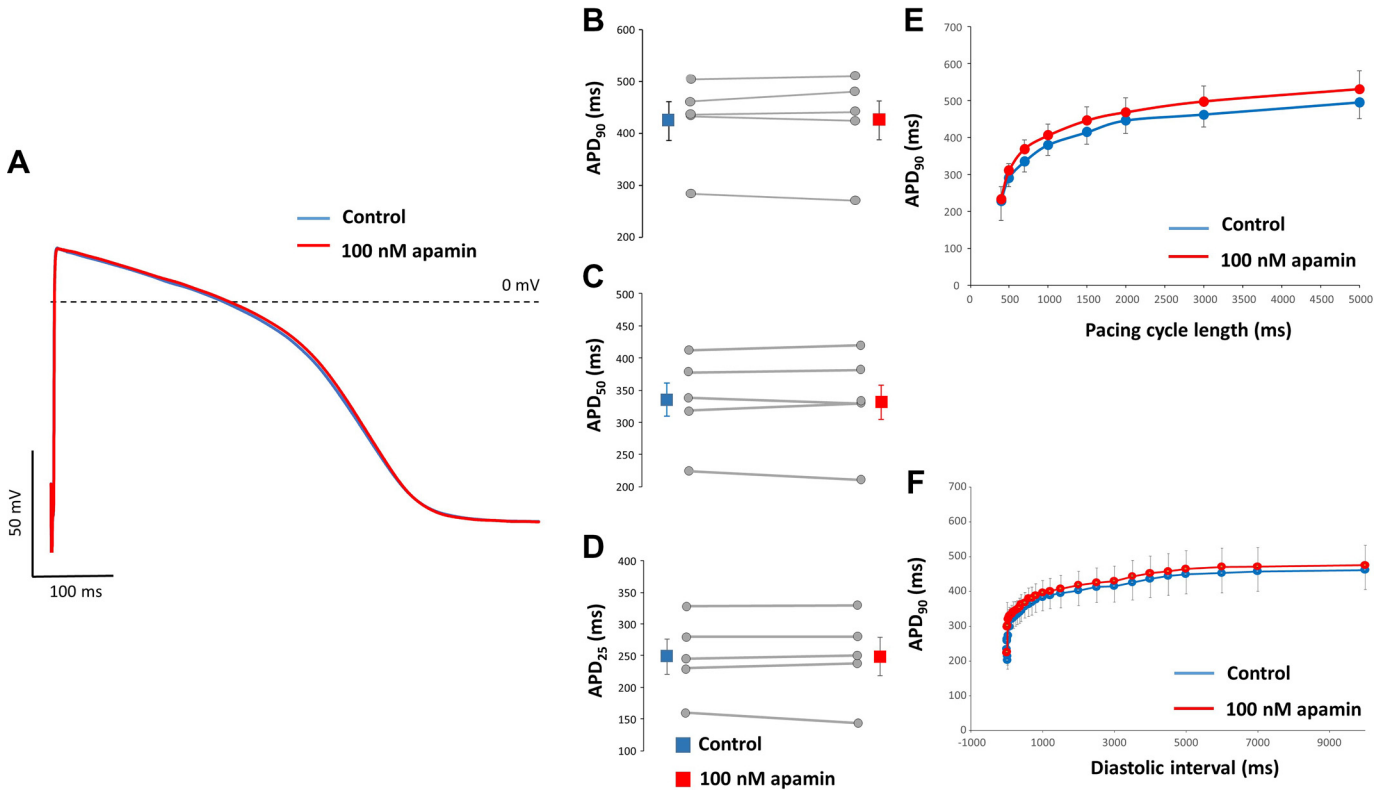

Figure 5. Effect of apamin on right ventricular trabeculae. *A*: representative traces of control (blue) and 100 nM apamin (red). *B–D*: action potential duration ($APD)_{90}$, 50 and 25 values of experiments under control and in the presence of 100 nM apamin. Control mean values are depicted in blue whereas apamin is marked with red circles. *E*: cycle length dependence of APD_{90} under control condition (blue graph) and in the presence of 100 nM apamin (red graph). *F*: standard S1-S2 restitution protocol of APD_{90} in control condition (blue) and after 100 nM apamin administration. *N* = 5 patients.

acquired using a Zeiss LSM 880 confocal microscope equipped with a C-Apochromat ×40/1.20 W Korr M27 objective in LineSequential mode. The pixel size was 0.35 μm/pixel, and a pixel dwell time of 4.12 μs was used, with line averaging set to 4. AF488 (SK2; Ex/Em = 488/523 nm) was detected within a range of 493–552 nm, and AF635 (Cav1.2; Ex/Em = 633/693 nm) was detected within the range of 640–747 nm. Additional image acquisition parameters are provided in the Supplemental Material. Immunostaining specificity was assessed using two negative controls: omission of the primary antibody and incubation with the primary antibody in the presence of the corresponding blocking peptide (SK2: 1:20, Alomone Labs, Cat. No. BLP-PC028; Cav1.2: 1:20, Alomone Labs, Cat. No. BLP-CC003). No primary and blocking peptide controls are presented in Supplemental Fig. S2. For each of the four hearts, three slices were imaged at separate fields, and three cardiomyocytes per field were analyzed and averaged. Colocalization was quantified by calculating Pearson correlation coefficients using the Coloc2 plugin in ImageJ (FIJI, v.1.54p).

Isolation of Cardiomyocytes from Failed Human Hearts

Ventricular myocytes were enzymatically dissociated from eight failed human hearts. A portion of the left ventricular wall was excised with an attached branch of the left descending coronary artery, which was cannulated and mounted on a modified 60-cm high Langendorff perfusion apparatus. Each preparation was perfused with each of the following perfusates for the times indicated: *1*) normal Tyrode's solutions, 10 min; *2*) Ca^{2+}-free Tyrode's solution, 10 min, and *3*) Ca^{2+}-free Tyrode's solution containing collagenase (type I, 0.66 mg/mL, Sigma-Aldrich Fine Chemicals),

Table 2. *APD parameters from right ventricular trabeculae at 1,000 ms pacing cycle length*

	APD_{90}		APD_{50}		APD_{25}	
	Control, ms	100 nM Apamin, ms	Control, ms	100 nM Apamin, ms	Control, ms	100 nM Apamin, ms
1	283	269	224	210	159	143
2	433	423	337	329	245	250
3	505	511	412	420	328	329
4	435	440	318	329	230	237
5	462	480	377	381	280	280
Mean (ms)	424.0	425.2	334.2	334.2	248.8	248.3
SEM (ms)	37.4	41.8	31.8	35.3	27.9	30.5

N = 5 patients. APD, action potential duration.

Table 3. *Cycle length-dependent APD_{90} changes in right ventricular trabeculae*

CL, ms	Control APD_{90} (Means ± SE, ms)	100 nM Apamin APD_{90} (Means ± SE, ms)
400	228 ± 42	233 ± 42
500	290 ± 23	310 ± 22
700	334 ± 35	369 ± 34
1,000	380 ± 42	406 ± 41
1,500	415 ± 45	447 ± 49
2,000	447 ± 50	469 ± 53
3,000	463 ± 46	498 ± 59
5,000	496 ± 59	532 ± 66

$N = 5$ patients. APD, action potential duration; CL, cycle length.

elastase (type III, 0.045 mg/mL, Sigma-Aldrich Fine Chemicals), taurine (50 mmol/L, Sigma-Aldrich Fine Chem-icals), and BSA (fraction V, fatty acid free, 2 mg/mL, Sigma-Aldrich Fine Chemicals), 15 min. After this series of perfusions, the dissociation solution was supplemented with protease (type XIV, 0.12 mg/mL, Sigma-Aldrich Fine Chemicals), and the tissue was perfused for an additional 45–60 min. Portions of clearly digested left ventricular wall were removed, minced into small pieces, and placed into either Kraft-Brühe (KB) solution or Ca^{2+}-free Tyrode's solution supplemented $CaCl_2$ (1.25 mmol/L) for 15 min. After this period, the suspension of minced tissue was gently agitated in a small beaker to obtain single cells. Throughout the isolation procedure, all solutions were oxygenated with 100% O_2 while their temperatures were maintained at 37°C. After a suspension of isolated myocytes was obtained, individual heart cells were allowed to settle to the bottom of the beaker for 10 min. Half of the supernatant was then replaced by fresh solution, and the cells resuspended in the solution were allowed to settle. This procedure was repeated three times to retard further enzymatic digestion. Myocytes in KB solution were stored at 4°C, and those stored in Tyrode's solution were maintained at 12°C to 14°C.

Cell isolation solutions.

The composition of each solution used for myocyte isolation was (in mmol/L) as follows: *1*) cardioplegic solution: NaCl 110, KCl 16, $MgCl_2$ 16, $CaCl_2$ 1.2, and $NaHCO_3$ 10; *2*) normal Tyrode's solution: NaCl 135, KCl 4.7, $NaHCO_3$ 4.4, KH_2PO_4 1.2, $MgSO_4$ 1.2, HEPES 10, glucose 10, and CaCl2 1.0 (pH 7.2 adjusted with NaOH); *3*) Ca^{2+}-free solution: NaCl 135, KCl 4.7, KH_2PO_4 1.2, $MgSO_4$ 1.2, HEPES 10, $NaHCO_3$ 4.4, and glucose 10 (pH 7.2 adjusted with NaOH); and *4*) KB solution: KOH 90, L-glutamic acid 70, taurine 15, KCl 30, KH_2PO_4 10, $MgCl_2$ 0.5, HEPES 10, glucose 11, and EGTA 0.5 (pH 7.3 adjusted with KOH).

Voltage-Clamp Measurements of the Potassium Current

One drop of the cell suspension was placed into a lucid chamber mounted on the stage of an inverted microscope (Olympus, Model IX71), and at least 10 min was allowed for myocytes to adhere before starting superfusion. External solution contained (in mM) NaCl 144, NaH_2PO_4 0.4, KCl 4.0, $CaCl_2$ 1.8, $MgSO_4$ 0.53, glucose 5.5, and HEPES 5.0 at a pH of 7.4. The solution contained 1 μM nisoldipine to inhibit L-type Ca^{2+} current. Micropipettes were fabricated from borosilicate glass capillaries (Clark Electromedical Instruments) using a microprocessor-controlled horizontal puller (Sutter Instruments). These electrodes had a resistance of 1.5–2.5 MΩ when filled with pipette solution containing (in mM): KCl 140, K_2ATP 5, HEPES 10, $MgCl_2$ 5, and GTP 0.1 and were titrated to pH 7.2 by using KOH. The free Ca^{2+} concentration in the pipette solution was set to 500 nM by using an appropriate mixture of EGTA and $CaCl_2$ (14). Currents were recorded with Axopatch 1-D amplifier (Axon Instruments) using whole cell configuration of the patch-clamp technique. Gigaseals were established with gentle suction, and the cell membrane beneath the tip was disrupted with further suction or by application of short electrical pulses. Membrane currents were digitized with an analog-to-digital converter (Digidata 1440A), under software control (pClamp 10.0). Membrane currents were recorded from each cell before and after application of 100 nM apamin, by using the whole cell configuration of the patch-clamp technique.

Statistics

Normal distribution of the data was verified by using Shapiro–Wilk test. Statistical significance ($P < 0.05$) was

Table 4. *APD_{90} changes during S1-S2 restitution in right ventricular trabeculae at 1,000 ms basic cycle length*

DI, ms	Control APD_{90} (Means ± SE, ms)	100 nM Apamin APD_{90} (Means ± SE, ms)	DI, ms	Control APD_{90} (Means ± SE, ms)	100 nM Apamin APD_{90} (Means ± SE, ms)
0	235 ± 46	224 ± 37	700	369 ± 32	381 ± 36
5	264 ± 46	228 ± 37	800	377 ± 32	389 ± 37
10	259 ± 69	299 ± 33	1,000	384 ± 34	397 ± 38
15	215 ± 28	303 ± 34	1,200	390 ± 35	402 ± 40
20	203 ± 20	303 ± 33	1,500	395 ± 36	408 ± 42
30	275 ± 22	321 ± 28	2,000	403 ± 38	419 ± 44
50	299 ± 24	327 ± 27	2,500	413 ± 41	426 ± 45
80	299 ± 23	331 ± 29	3,000	416 ± 41	430 ± 45
130	321 ± 23	336 ± 28	3,500	426 ± 44	444 ± 49
180	324 ± 23	343 ± 30	4,000	437 ± 47	453 ± 53
250	331 ± 24	347 ± 30	4,500	445 ± 48	458 ± 54
300	335 ± 25	350 ± 30	5,000	449 ± 49	466 ± 55
350	340 ± 23	355 ± 32	6,000	453 ± 51	471 ± 56
400	345 ± 26	364 ± 32	7,000	458 ± 52	472 ± 56
500	357 ± 29	368 ± 34	10,000	462 ± 54	476 ± 55
600	362 ± 30	381 ± 34			

$N = 5$ patients. APD, action potential duration; DI, diastolic interval.

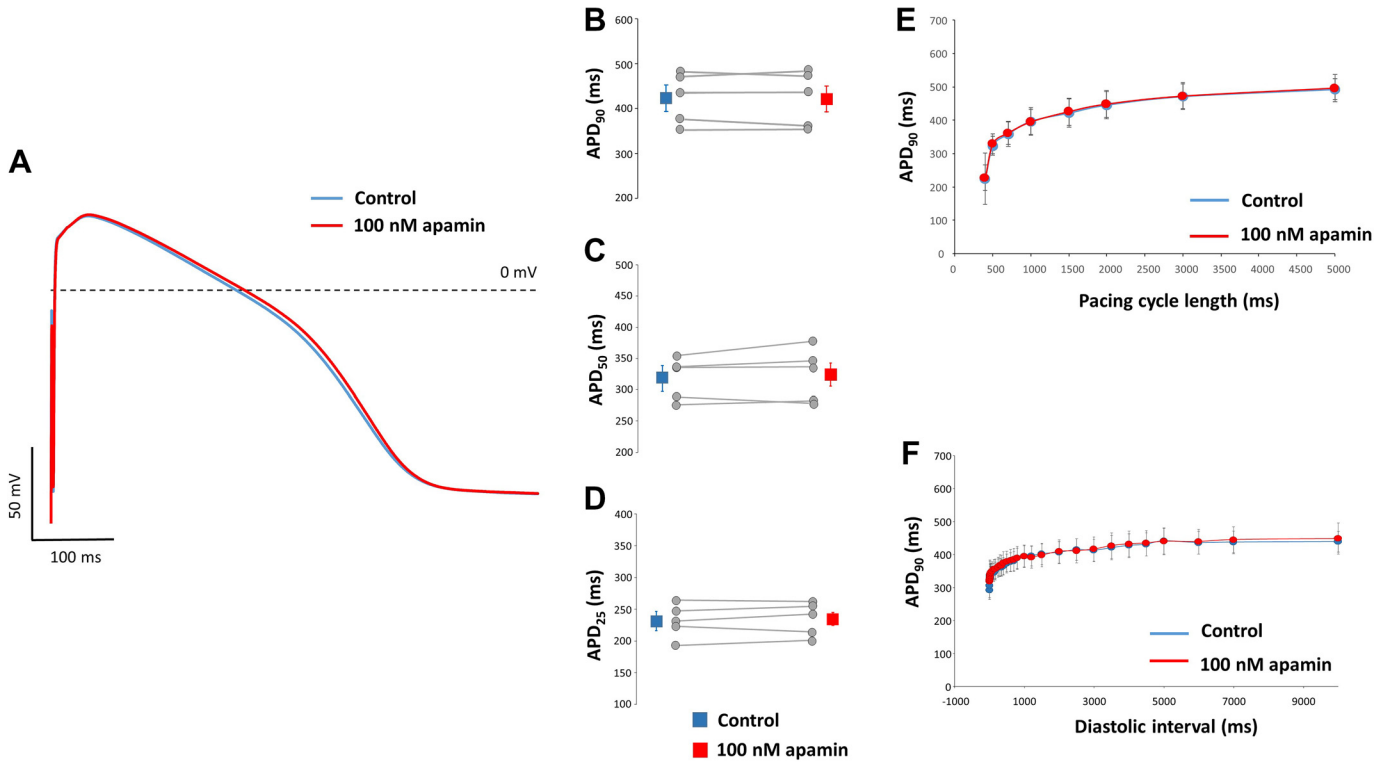

Figure 6. Effect of apamin on left ventricular trabeculae. *A*: representative traces of control (blue) and 100 nM apamin (red). *B–D*: action potential duration $(APD)_{90}$, 50, and 25 values of experiments under control and in the presence of 100 nM apamin. Control mean values are depicted in blue whereas apamin is marked with red circles. *E*: cycle length dependence of APD_{90} under control condition (blue graph) and in the presence of 100 nM apamin (red graph). *F*: standard S1-S2 restitution protocol of APD_{90} in control condition (blue) and after 100 nM apamin administration. $N = 5$ patients.

assessed using Student's *t* test. Data are presented as ±SE. In this study, "*N*" indicates the number of hearts and "*n*" reports the total number of technical replicates in the experiment. Throughout the study, we applied a hierarchical analysis; that is, all technical replicates derived from the same biological replicate were averaged.

RESULTS

Comparison of Undiseased and Failed Right Ventricular Action Potentials

The action potentials were obtained from right ventricular papillary muscles or trabecules. The undiseased preparations exerted markedly shorter APD values (APD_{90}: 256 ± 6 ms vs. 424 ± 37 ms, $P < 0.05$; APD_{50}: 192 ± 5 ms vs. 334 ± 31 ms, $P < 0.05$; APD_{25}: 130 ± 5 ms vs. 248 ± 27 ms, $P < 0.05$, $N =$ 19-5, respectively) (Fig. 1, *A* and *B*). The resting membrane potential was slightly, however statistically significantly depolarized in failed hearts (−84 ± 1 mV vs. −77 ± 9 mV, $P <$ 0.05, $N =$ 19-5 respectively). The phase 0 amplitude was identical between undiseased and failed hearts (108 ± 2 mV vs. 113 ± 3 mV, $n = 19$-8); however, the maximal speed of the depolarization considerably decreased in failed hearts (262 ± 21 V/s vs. 151 ± 32 V/s, $P < 0.05$, $N = 19$-5). Also, action potentials obtained from failing hearts did not show phase 1 repolarization. Independent *t* test was used for statistical comparison.

Comparison of Different Tissue Regions of Failed Human Ventricle

The main parameters of the right and left endocardial and left midmyocardial action potentials obtained from

Table 5. *APD parameters from left ventricular trabeculae at 1,000 ms pacing cycle length*

	APD_{90}		APD_{50}		APD_{25}	
	Control, ms	100 nM Apamin, ms	Control, ms	100 nM Apamin, ms	Control, ms	100 nM Apamin, ms
1	351	353	275	282	192	201
2	470	482	354	376	230	241
3	434	436	336	346	246	254
4	481	471	335	336	263	261
5	375	360	288	278	222	213
Mean, ms	422.9	420.9	318.3	324.1	231.3	234.5
SE, ms	29.6	29.0	20.4	18.7	15.1	10.3

$N = 5$ patients. APD, action potential duration.

Table 6. *Cycle length-dependent APD_{90} changes in left ventricular trabeculae*

CL, ms	Control APD_{90} (Means ± SE, ms)	100 nM Apamin APD_{90} (Means ± SE, ms)
400	224 ± 76	227 ± 38
500	324 ± 27	329 ± 29
700	358 ± 37	361 ± 33
1,000	397 ± 41	395 ± 38
1,500	422 ± 42	425 ± 40
2,000	445 ± 40	448 ± 40
3,000	471 ± 37	472 ± 40
5,000	492 ± 31	496 ± 40

$N = 5$ patients. APD, action potential duration; CL, cycle length.

failed human hearts were compared (Fig. 2, *A–D*). It was found that APD values did not show significant difference at none levels (APD_{90}: 424 ± 37 ms vs. 422 ± 29 ms vs. 524 ± 71 ms; APD_{50}: 332 ± 25 ms vs. 318 ± 20 ms vs. 397 ± 47 ms; APD_{25}: 248 ± 23 ms vs. 231 ± 15 ms vs. 298 ± 28 ms (N = 5-5-3, respectively). One-way ANOVA was used for statistical analysis.

Evaluation of SK2 Protein Expression

Expression of SK proteins was determined in left ventricular tissues from undiseased and failing hearts. No significant differences in SK1 (0.70 ± 0.10 vs. 0.95 ± 0.09), SK2 (1.04 ± 0.13 vs. 0.90 ± 0.12), and SK3 (0.80 ± 0.15 vs. 0.79 ± 0.16) expression were observed between the two groups (N = 5, n = 2, Student's t test, Fig. 3, *A–C*).

Effect of 100 nM Apamin on Membrane Current on Isolated Left Ventricular Failing Heart

Total membrane current was measured from a holding potential of −80 mV. Rectangular voltage steps between −80 mV and 60 mV having 10 mV increments were used to obtain the current-voltage relationship. The intracellular Ca^{2+} was set to 500 nM by using an appropriate mixture of EGTA and $CaCl_2$ to activate I_{SK}. Then, 100 nM apamin was used to dissect apamin-sensitive current. However, apamin did not change the control current at any membrane potential (n = 4, N = 4, paired t test, Fig. 4, *A–C*).

Effect of 100 nM Apamin in Right Ventricular Papillary Muscles Obtained from Failing Human Heart

Effect of 100 nM apamin, which is considered as a specific inhibitor of SK channels, was investigated in right ventricular papillary muscles and trabeculae at a basic cycle length of 1,000 ms. Apamin exerted no effect at repolarization level of APD_{25} (248 ± 27 ms vs. 248 ± 30 ms; n = 8, N = 5, paired t test), at APD_{50} (334 ± 31 vs. 334 ± 35 ms; N = 5; paired t test), and at APD_{90} (424 ± 37 vs. 425 ± 41 ms; n = 8 N = 5; paired t test, Fig. 5, *A–D*, Table 2). Cycle length-dependent effect was also investigated between 400 and 5,000 ms at APD_{90}, however, 100 nM failed to change APD at any cycle length (Fig. 5*E*, Table 3). Similarly, restitution curves were identical between control and 100 nM apamin-treated preparations (Fig. 5*F*, Table 4).

Effect of 100 nM Apamin on Left Ventricular Trabeculae Obtained from Failing Human Heart

Effect of 100 nM apamin was investigated in left ventricular trabeculae at a basic cycle length of 1,000 ms. After the control condition, 100 nM apamin was employed. The intervention exerted no effect at any repolarization level (APD_{90}: 422 ± 29 →420 ± 29 ms; APD_{50}: 318 ± 20 →324 ± 18 ms; APD_{25}: 231 ± 15 →234 ± 10 ms, n = 5, N = 5, paired t test, Fig. 6, *A–D*, Table 5). Cycle length-dependent behavior and S1-S2 restitution were identical between control and apamin (Fig. 6, *E* and *F*, Tables 6 and 7).

Effect of 100 nM Apamin on Left Ventricular Midmyocardial Tissue Slices Obtained from Failing Human Heart

Midmyocardial tissue slices (400 μm) were used for the measurements. Similarly to the previous experiments, 100 nM apamin failed to change AP characteristics (APD_{90}: 524 ± 71 →513 ± 70 ms; APD_{50}: 397 ± 47 →386 ± 41 ms; APD_{25}: 298 ± 28 →278 ± 11 ms, n = 4, N = 3, paired t test, Fig. 7, *A–D*, Table 8).

Effect of 5 μM NS-309 and 100 nM Apamin on Left Midmyocardial Slices

The effect of SK-channel activator NS-309 was investigated in left ventricular endocardial preparations. After

Table 7. *APD_{90} changes during S1-S2 restitution in left ventricular trabeculae at 1,000 ms basic cycle length*

DI, ms	Control APD_{90} (Means ± SE, ms)	100 nM Apamin APD_{90} (Means ± SE, ms)	DI, ms	Control APD_{90} (Means ± SE, ms)	100 nM Apamin APD_{90} (Means ± SE, ms)
0	292 ± 27	319 ± 27	700	380 ± 29	384 ± 33
5	306 ± 37	323 ± 27	800	389 ± 30	389 ± 35
10	334 ± 45	324 ± 28	1,000	394 ± 31	395 ± 34
15	337 ± 45	329 ± 27	1,200	396 ± 30	392 ± 32
20	326 ± 42	334 ± 29	1,500	402 ± 31	398 ± 34
30	331 ± 41	341 ± 29	2,000	406 ± 32	409 ± 36
50	339 ± 26	345 ± 28	2,500	414 ± 33	411 ± 36
80	345 ± 26	349 ± 29	3,000	412 ± 33	416 ± 36
130	346 ± 26	355 ± 29	3,500	420 ± 36	427 ± 39
180	350 ± 26	356 ± 29	4,000	427 ± 35	432 ± 38
250	361 ± 25	361 ± 30	4,500	431 ± 34	434 ± 38
300	360 ± 27	367 ± 32	5,000	441 ± 39	439 ± 40
350	361 ± 25	366 ± 32	6,000	435 ± 34	439 ± 36
400	364 ± 26	374 ± 34	7,000	437 ± 34	445 ± 39
500	372 ± 28	379 ± 30	10,000	439 ± 31	448 ± 47
600	377 ± 29	382 ± 33			

N = 5 patients. APD, action potential duration; DI, diastolic interval.

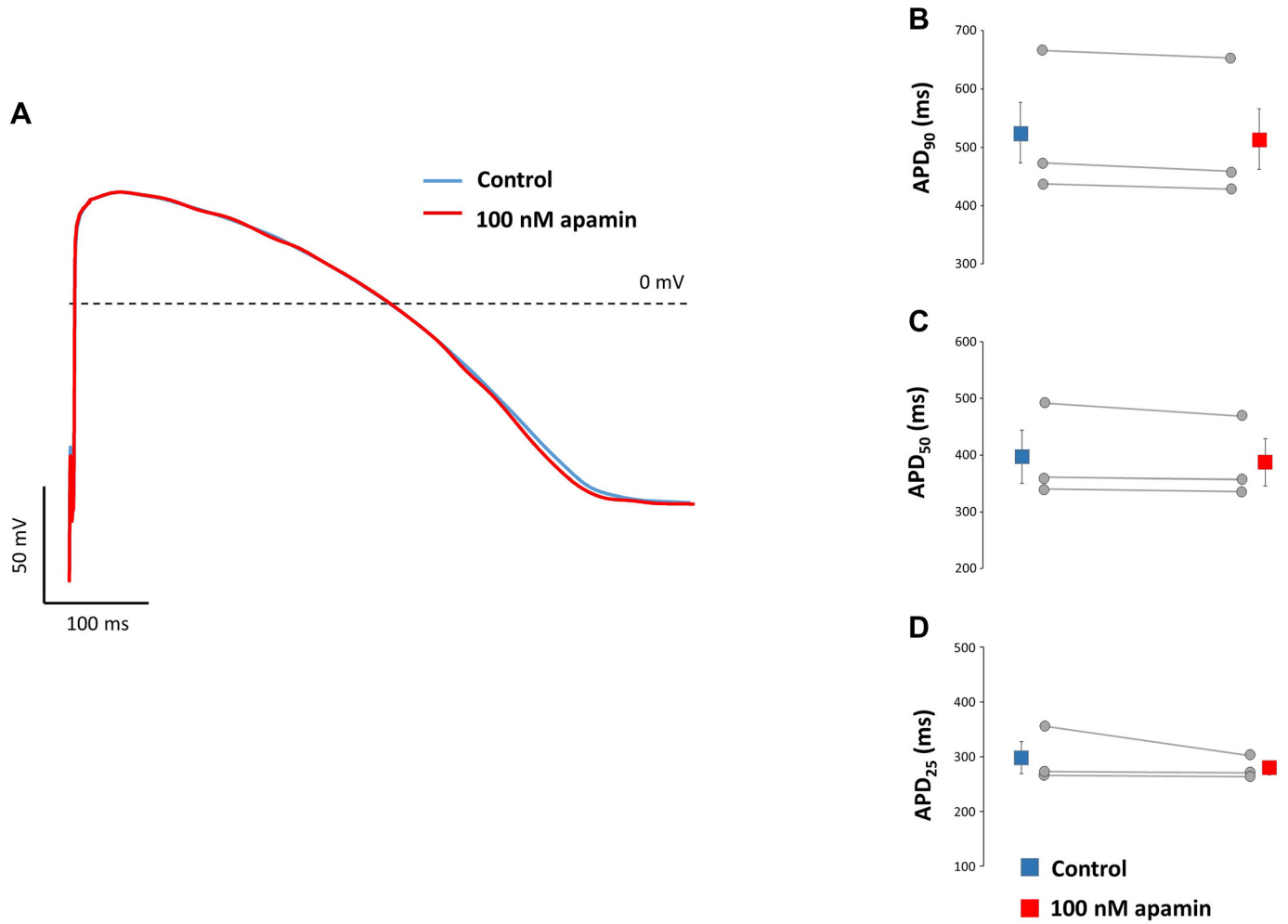

Figure 7. Effect of apamin on left midmyocardial tissue slices. *A*: representative traces of control (blue) and 100 nM apamin (red). *B–D*: the action potential duration $(APD)_{90}$, 50, and 25 values of experiments under control and in the presence of 100 nM apamin. Control mean values are depicted in blue whereas apamin is marked with red circles. $N = 3$ patients.

control recordings (APD_{90}: 441 ± 19 ms), 5 μM NS-309 shortened the action potential (APD_{90}: 421 ± 20* ms) and this effect was reverted by 100 nM apamin (APD_{90}: 439 ± 17# ms; $N = 6$, $n = 9$, $*P < 0.05$ control vs. NS-309, $\#P < 0.05$ NS-309 vs. apamin, one-way repeated-measures ANOVA and Bonferroni–Holm post hoc test Fig. 8, *A* and *B*, Table 9).

Effect of 100 nM Apamin following 200 nM Isoproterenol

Application of 200 nM isoproterenol shortened the action potential in 1,000 ms basic cycle length (483 ± 13 ms → 405 ± 14 ms, $P < 0.05$), however, the subsequently applied apamin failed to further prolong the action potential (412 ± 14, $P = 0.11$, one-way repeated-measures ANOVA and Bonferroni–Holm post hoc test, $n = 9$, $N = 5$, Fig. 9, *A–C*). This experimental condition was tested across a range of cycle lengths from 400 to 5,000 ms; however, apamin did not alter APD_{90} at any cycle lengths (Tables 10 and 11).

In a separate set of experiments, the effect of 10 nM dofetilide was examined (Fig. 9, *D* and *E*) to assess repolarization reserve. Under these conditions, dofetilide markedly prolonged the action potential duration even at a BCL of 1,000 ms, resulting in incomplete repolarization at this pacing cycle length ($n = 4$, $N = 4$).

Table 8. *Action potential APD parameters from left midmyocardial slices at 1,000 ms pacing cycle length*

	APD_{90}		APD_{50}		APD_{25}	
	Control, ms	100 nM Apamin, ms	Control, ms	100 nM Apamin, ms	Control, ms	100 nM Apamin, ms
1	665	652	491	469	356	302
2	472	459	360	356	273	271
3	436	428	340	335	266	263
Mean, ms	524.7	513.2	397.2	386.9	298.5	278.9
SE, ms	71.0	70.1	47.3	41.6	28.9	11.9

$N = 3$ patients. APD, action potential duration.

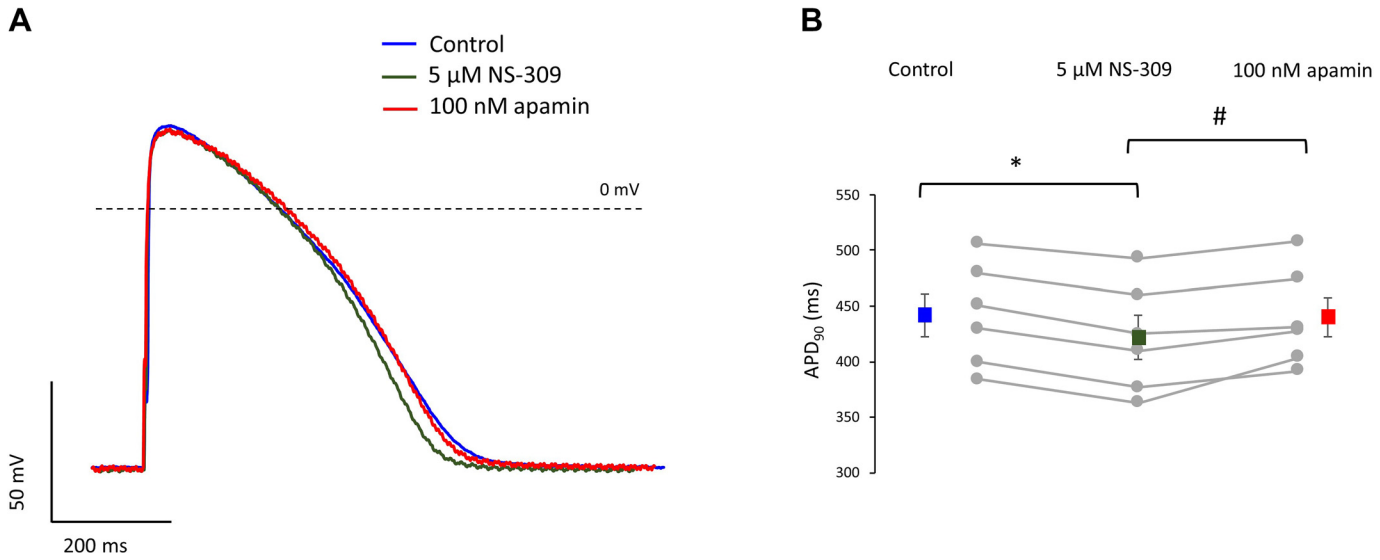

Figure 8. Effect of small-conductance Ca^{2+}-activated K^+ (SK)-channel activation and inhibition on failing human hearts. *A*: representative action potential traces obtained from left ventricular failing hearts under control condition (blue trace), after 5 µM NS-309 (green trace), and finally 100 nM apamin (red trace). *B*: individual as well as mean action potential duration (APD)90 values of each experiments under control, 5 µM NS-309, and 100 nM apamin application. *N* = 6 patients.

SK2 and Cav1.2 Colocalization in the Failing Human Heart

SK2 and Cav1.2 colocalization was examined in left ventricular tissues of failing hearts. Pearson's correlation coefficient showed only a moderate positive correlation between SK2 and Cav1.2 expression (means ± SE: 0.43 ± 0.03; Fig. 10, *A* and *B*). Data are presented as median with interquartile range.

DISCUSSION

In the present study, we identified a functional dissociation between SK channel expression and electrophysiological contribution in the terminal failing human ventricle. Although SK protein is expressed in failing myocardium, selective inhibition with 100 nM apamin did not modify ventricular action potential morphology at any pacing rate, and no apamin-sensitive current could be resolved in isolated human ventricular myocytes. Together, these findings indicate that, despite preserved molecular presence, SK channels do not provide a measurable contribution to repolarizing current in end-stage human heart failure.

Table 9. *APD_{90} changes upon SK channel activation (5 µM NS-309) and inhibition (100 nM apamin)*

	Control APD_{90}, ms	5 µM NS-309 APD_{90}, ms	100 nM Apamin APD_{90}, ms
1	384	363	404
2	480	460	475
3	400	377	392
4	451	425	431
5	506	493	508
6	430	410	428
Mean, ms	441.8	421.4	439.7
SE, ms	19.1	20.2	18.0

N = 6 patients. APD, action potential duration; SK, small-conductance Ca^{2+}-activated K^+.

Electrophysiological Remodeling of Action Potential in Chronic Heart Failure

A large number of animal models aimed to characterize electrophysiological alterations in heart failure. Although the technical approaches show large variability, there are some coherent findings among the results. Principally, the action potential duration of failing hearts is generally found to be prolonged in different models (15–18), and we found similar changes in the present study that could be due to downregulation of I_{to}, I_{Kr}, and I_{Ks} and upregulation of I_{NaL} (15, 16, 18–20). Lengthening of the action potential provides longer Ca^{2+}-influx through the L-type Ca^{2+} channels that may augment available Ca^{2+} and may improve ventricular performance (21), however, it could also favor early afterdepolarization (EAD) formation (22). Nevertheless, in this study, EAD development was not observed at either normal or slow (5,000 ms) pacing cycle lengths. The most established transmembrane current showing downregulation is the I_{to}: several animal (16, 17, 23, 24) and human (19, 25, 26) studies claimed I_{to} downregulation via reduced Kv4.3 mRNA and protein (23) and consequential disappearance of the notch (27). In agreement with these observations, in this study, all preparations from all regions (i.e., endocardial or midmyocardial tissue layers) exhibited action potentials without phase 1 repolarization, suggesting a coherent I_{to} downregulation similarly to a previous study in human failing hearts (9). Interestingly, in the present paper, there were no large differences between endocardial and midmyocardial APD_{90} values indicating moderate transmural APD gradient, in line with a previous paper on human heart failure (28). Downregulation of I_{K1} has also been reported in heart failure (23). Consistent with this, the resting membrane

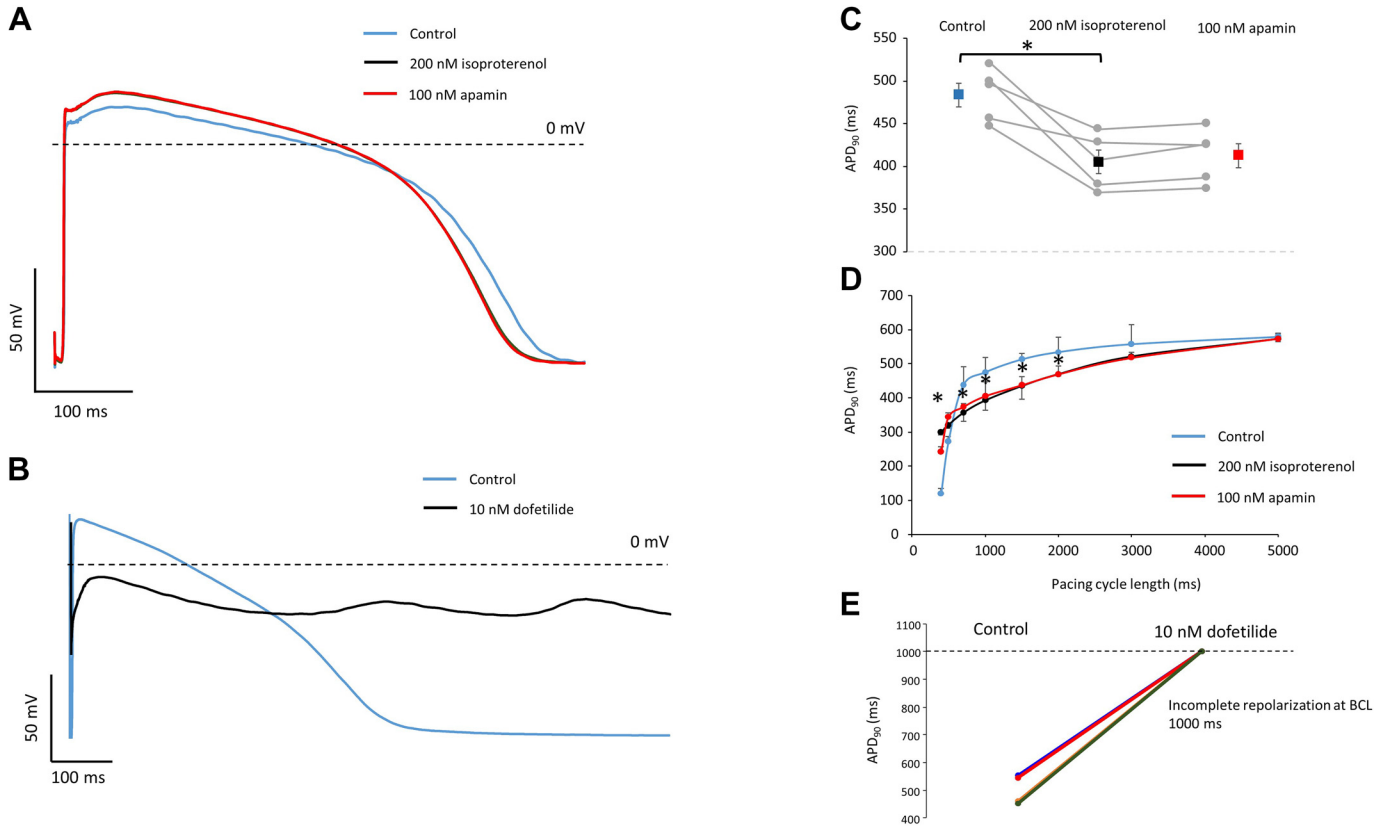

Figure 9. Effect of small-conductance Ca^{2+}-activated K^+ (SK)-channel inhibition after β-adrenergic activation. *A*: original representative action potential traces recorded from left ventricular failing hearts under control condition (blue trace), after application of 200 nM isoproterenol (black trace) and after 100 nM apamin (red trace). *B*: the individual experiments and corresponding means. *C*: the cycle length dependent effects of 200 nM isoproterenol and 100 nM apamin. *D*: the effect of 10 nM dofetilide (black trace) on left ventricular human action potentials and corresponding individual experiments (*E*). *N* = 5 patients.

potential in the present study was slightly depolarized compared with that of normal heart.

It is important to note that in this study, all action potentials were measured by the conventional microelectrode technique from intact tissue slices. This approach avoids the limitations associated with enzymatic dissociation, such as excessively prolonged action potentials, increased frequency-dependent behavior, and increased susceptibility to any intervention. This is well demonstrated by the fact that the average frequency-corrected QT interval on the ECG of the patients was 494 ± 14 ms, whereas the mean action potential duration in the midmyocardial layer was 511 ± 52 ms, indicating that these preparations accurately reflect the pathophysiological condition.

Table 10. *APD_{90} changes upon beta-adrenergic activation (200 nM isoproterenol) and SK channel inhibition (100 nM apamin)*

	Control APD_{90}, ms	200 nM ISO APD_{90}, ms	100 nM Apamin APD_{90}, ms
1	495	443	450
2	456	428	425
3	446	369	374
4	520	407	426
5	500	379	387
Mean, ms	483.9	405.3	412.5
SE, ms	13.9	14.1	14.0

N = 5 patients. APD, action potential duration; CL, pacing cycle length; SK, small-conductance Ca^{2+}-activated K^+.

Putative Characteristics of SK-Current and Effect of Its Inhibition

Molecular biological experiments of the present work demonstrated weak but unequivocal expression of the SK2 channel in both undiseased and failing hearts, however, our results did not confirm the previously reported SK2 channel upregulation in human heart failure (7, 29), i.e., SK-channel density was identical in human undiseased and failing hearts. The reasons for the observed discrepancy between the results are unknown. The gender composition, mean age, and pathogenesis of heart failure seemingly did not differ significantly between the patients involved in previous papers and the present study. In contrast, the shape of the action potentials reported in this study and in papers investigating human failing action potentials is markedly different: Bonilla et al. (7) and Chang et al. (29) illustrated action potentials with I_{to} and notch, whereas Yu et al. (9) and the present study reported lack of phase 1 repolarization and notch. This characteristic and presumably important discrepancy of action potential configuration draws attention to potentially important differences in electrical remodeling that could be due to the rather diverse etiology of heart failure, or medical history (comorbidities) of the patients. In the present study,

Table 11. *Cycle length-dependent APD_{90} changes upon beta-adrenergic activation (200 nM isoproterenol) and SK channel inhibition (100 nM apamin)*

CL, ms	Control APD_{90} (Means ± SE, ms)	200 nM ISO APD_{90} (Means ± SE, ms)	100 nM Apamin APD_{90} (Means ± SE, ms)
400	118 ± 26	299 ± 3	241 ± 28
500	272 ± 66	319 ± 2	342 ± 18
700	436 ± 13	355 ± 4	372 ± 15
1,000	474 ± 16	391 ± 5	404 ± 22
1,500	511 ± 21	434 ± 6	436 ± 29
2,000	533 ± 24	469 ± 8	468 ± 32
3,000	556 ± 26	521 ± 15	516 ± 35
5,000	578 ± 26	573 ± 28	573 ± 51

$N = 5$ patients. APD, action potential duration.

inhibition of SK channels by apamin had no effect on either the ionic current or the action potential, similarly to our previous study where apamin failed to lengthen the undiseased human action potential (3). In contrast, Bonilla et al. (7) demonstrated ~20% lengthening of the action potential duration (APD) at the 90% repolarization level following the administration of 100 nM apamin in human failing myocytes. Similarly, Yu et al. (9) investigated human failing hearts using optical mapping and found that apamin increased the action potential duration by ~10%. Chang et al. (29) reported an 11% effect with apamin and also compared SK2 current in both undiseased and failing hearts (29). In that study, the median SK2 current density was 4.22 pA/pF in failing hearts and 0.98 pA/pF in the nonfailing group at 0 mV with 1 μM internal Ca^{2+}. These values are notably high, since a previous study from our laboratory investigated repolarizing currents in the undiseased human heart (30) and it was observed that the main repolarizing current, I_{Kr}, in undiseased human midmyocardial cells was less than 0.3 pA/pF when measured under an action potential command (30). Also, the peak I_{K1} in undiseased human ventricular myocytes at −60 mV was less than 1 pA/pF (30) (Table 12).

SK Current Is Weakly Activated in End-Stage Heart Failure

It is important to note that in this study, when SK channels were activated by NS-309, preparations responded with slight action potential shortening that was reversed by subsequently applied apamin. The NS-309-induced shortening of the action potential was modest (~4.5%), which in principle suggests a trend toward an antiarrhythmic effect; however, given the small magnitude of this effect, its clinical relevance remains questionable. NS-309 is known as a positive gating modulator, i.e., shifts the Ca^{2+}-activation curve toward lower values (31). Furthermore, another paper has shown that in calmodulin mutants causing unstable association with calmodulin binding site of the channel, NS-309 was able to stabilize the calmodulin-channel interaction (32), which may have crucial importance since SK-channels are not directly regulated by the intracellular Ca^{2+} but via Ca^{2+}-calmodulin interaction in the calmodulin-binding domain in the C-terminus of the channel (33–36). Furthermore, it was also shown that calmodulin regulates the assembly and surface expression of the channel (35). Therefore, NS-309 demonstrates the "latent capacity" of SK channels, but simultaneously indicates that under baseline conditions (i.e., without any pharmacological intervention) these channels are not sufficiently activated to influence repolarization.

The importance of the calmodulin-channel interaction is further underscored by the observation that the β-agonist isoproterenol, although it markedly shortened the action potential—an effect partly attributable to enhanced I_{CaL} inactivation secondary to increased Ca^{2+} release—was nevertheless unable to augment the effect of apamin. Thus, it appears that in the failing heart, the relatively lower intracellular Ca^{2+} level is not the sole determinant of the functional "silencing" of SK channels.

Mechanistic Insights into SK Channel Dysfunction

It is a challenging question why SK2 channels, although expressed in the membrane, appear to be functionally silent. Since the Ca^{2+} sensitivity of these channels is not direct but mediated through accessory proteins, one plausible explanation is that the Ca^{2+}-calmodulin complex is not sufficiently stable to effectively activate the channel; this interpretation is also supported by our experiments with NS-309 and previous study (32). Furthermore, it was shown that the colocalization of L-type Ca^{2+} channels and SK2 channels is

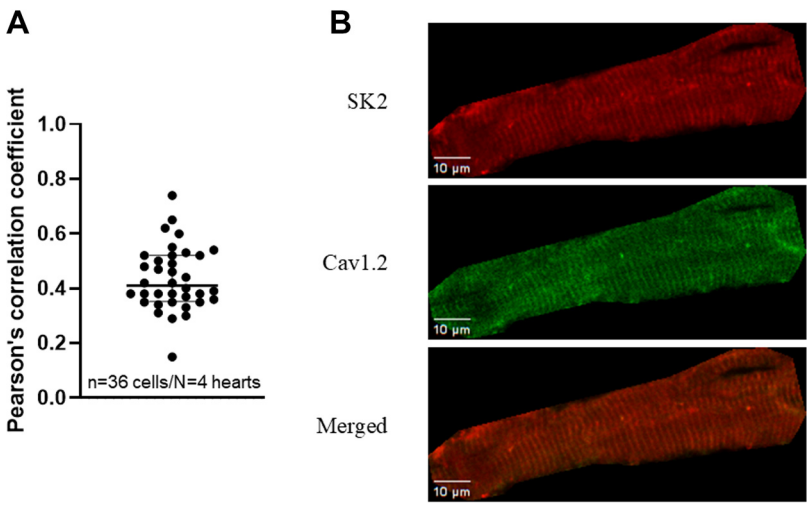

Figure 10. Small-conductance Ca^{2+}-activated K^+ SK2 and Cav1.2 colocalization in the left ventricles of failing hearts. Colocalization was measured by simultaneous fluorescent labeling. SK2 and Cav1.2 showed only a moderate colocalization, as determined by Pearson's correlation coefficient (*A*). Representative images of SK2 (red), Cav1.2 (green), and the merged signal are shown in *B*. For each of the four hearts, three slices per heart and three cardiomyocytes per slice were analyzed and averaged. Data are presented as median with interquartile range.

Table 12. *Summary of apamin induced action potential effect on human heart failure preparations*

	Species	State	Region	Object	Technique for AP Measurements	Apamin Effect (%)	Apamin Concentration, nM
Bonilla et al. (7)	Human	HF	LV	Isolated cells	Perforated patch-clamp	20	100
Chang et al. (29)	Human	HF	LV	Isolated cells	Whole cell patch-clamp	11	100
Yu et al. (9)	Human	HF	LV	Tissue	Wedge preparation	10	100

HF, heart failure; LV, left ventricle.

important for their activation during the action potential (37), and this coupling was markedly reduced in the present study. Consequently, the activating Ca^{2+} signal may be unable to generate a functionally significant current during the action potential, even in the presence of isoproterenol.

It is also important to emphasize that in this study, SK channel expression was not upregulated compared with healthy ventricular myocardium, where the SK channel contribution to the repolarization is marginal (3, 38–40). The combined effect of these alterations may therefore result in a functional impairment of the channel in the hearts we investigated.

Highly Vulnerable Repolarization in End-Stage Heart Failure

Importantly, 10 nM dofetilide, a concentration close to its IC_{50}, prolonged the action potential duration to such an extent at 1,000 ms cycle length that full repolarization could not be achieved, rendering the tissue unexcitable. For comparison, a fivefold higher concentration of dofetilide produces only ~30% prolongation of APD in healthy donor ventricular myocardium (41), where repolarization reserve is intact. This finding suggests that in terminal heart failure, both I_{Kr} and other currents contributing to repolarization reserve (I_{Ks}, I_{K1}, I_{to}) are downregulated or functionally reduced, in line with previously published data (42). This observation further supports the notion that a substantial SK current—at least not to an extent that would be sufficient to rescue repolarization from excessive dofetilide-induced effects—is unlikely to play a significant role in repolarization in end-stage failing hearts.

What Could Explain the Divergent Findings?

Yu et al. (9) compared the relative importance of SK-current with I_{Kr} and I_{Ks} in the failing human heart by using optical mapping at 2,000 ms pacing cycle length. It was found that apamin prolonged the action potential by 10% whereas the subsequently applied 50 μM chromanol caused further 17% prolongation then further 100 nM E-4031 increased action potential duration by 35%. This suggests that in the failing hearts they studied, remodeling may have been less advanced, with other repolarization reserve currents still functionally present.

In contrast, in the terminal stage heart failure with reduced ejection fraction (HFrEF) hearts examined in our study, reserve currents appear to be largely lost, as even low-dose I_{Kr} inhibition resulted in incomplete repolarization. It is therefore plausible that more advanced, end-stage remodeling accounts for the differences between studies, highlighting the importance of disease stage in samples from failing human hearts.

Thus, our findings do not exclude the possibility that in earlier phases of heart failure (or different etiology of the disease) SK channels may still participate in repolarization. However, as the remodeling progresses, they appear to become functionally ineffective, together with other reserve currents.

An additional study demonstrated that only homomeric SK2 channels are sensitive to apamin, whereas heteromeric SK2-SK3 channels are less sensitive (43). This raises the question of how channel composition varies from patient to patient in human heart failure, which may influence the effect of apamin.

In summary, the complex regulation of SK channels, the various influencing factors, and the inherent variability in remodeling during heart failure may explain why the contribution of SK-current to repolarization is inconsistent and not uniform across all investigated patient populations.

Conclusions

The observations in the present study raise questions regarding the exact role of SK current in ventricular repolarization in the pathological setting of human heart failure, and further studies are needed to fully elucidate this issue.

DATA AVAILABILITY

All data generated or analyzed during this study are included in this published article.

SUPPLEMENTAL MATERIAL

Supplemental Fig. S1: https://doi.org/10.5281/zenodo.19704528.
Supplemental Fig. S2: https://doi.org/10.5281/zenodo.19704528.

GRANTS

This work was supported by the National Research Development and Innovation Office Grants NKFIH K 135464, K 142738, ADVANCED 150395, GINOP-2.3.2.-15-2016-00006, and GINOP-2.3.2.-15-2016-00047 (to A.V. and N.J.); FK-142949 (to N.N. and Z.K.); STARTING-150884 (to Z.K.); K-147212, GINOP-2.3.2.-15-2016-00040, and TKP2021-EGA-32 (to I.B.), the Ministry of Human Capacities Hungary Grant EFOP-3.6.2-16-2017-00006 (to A.V., N.J., and I.B.), the Albert Szent-Györgyi Medical School institutional grant SZTE AOK-KKA 2021 (to L.V.), SZTE AOK-KKA 2022 (to N.J.) and SZTE AOK-KKA 2024 (to I.B.) and by Hungarian Research Network HUN-REN TKI project (to Z.K., A.V., and N.J.). This study was also supported by Project RRF-2.3.1-21-2022-00003 "National Heart Laboratory, Hungary" implemented with the support provided by the European Union (to I.B. and B.M.) and by the Pharmaceutical and Medical Device Developments Competence Centre of the Life Sciences Cluster of the Centre of Excellence for Interdisciplinary Research, Development and Innovation of the University of Szeged,

Hungary. The study was further supported by the Hungarian Academy of Sciences János Bolyai Scholarship (to Z.K.). The study was further supported by the University of Szeged Open Access Fund, Grant ID: 8680.

DISCLOSURES

No conflicts of interest, financial or otherwise, are declared by the authors.

AUTHOR CONTRIBUTIONS

A.S.A.M., T.R., M.B., I.B., A.V., B.M., and N.N. conceived and designed research; A.S.A.M., V.D.-H., A.A.E.A., L.T., N.M., G.M., B.P., G.B., Z.K., K.B., A.A.S., T.R., M.B., L.V., and N.N. performed experiments; A.S.A.M., V.D.-H., L.T., N.M., Z.K., K.B., L.V., N.J., and N.N. analyzed data; A.S.A.M., V.D.-H., L.T., N.M., L.V., N.J., A.V., B.M., and N.N. interpreted results of experiments; A.S.A.M., V.D.-H., L.T., and N.N. prepared figures; A.S.A.M., V.D.-H., L.T., and N.N. drafted manuscript; A.S.A.M., T.R., M.B., L.V., N.J., I.B., A.V., B.M., and N.N. edited and revised manuscript; A.S.A.M., V.D.-H., L.T., N.M., G.M., B.P., G.B., Z.K., K.B., A.A.S., T.R., M.B., L.V., N.J., I.B., A.V., B.M., and N.N. approved final version of manuscript.

REFERENCES

1. **Xu Y**, **Tuteja D**, **Zhang Z**, **Xu D**, **Zhang Y**, **Rodriguez J**, **Nie L**, **Tuxson HR**, **Young JN**, **Glatter KA**, **Vazquez AE**, **Yamoah EN**, **Chiamvimonvat N.** Molecular identification and functional roles of a Ca^{2+}-activated K^+ channel in human and mouse hearts. *J Biol Chem* 278: 49085–49094, 2003. doi:10.1074/jbc.M307508200.
2. **Eisner DA**, **Vaughan-Jones RD.** Do calcium-activated potassium channels exist in the heart? *Cell Calcium* 4: 371–386, 1983. doi:10.1016/0143-4160(83)90015-5.
3. **Nagy N**, **Szuts V**, **Horvath Z**, **Seprenyi G**, **Farkas AS**, **Acsai K**, **Prorok J**, **Bitay M**, **Kun A**, **Pataricza J**, **Papp JG**, **Nanasi PP**, **Varro A**, **Toth A.** Does small-conductance calcium-activated potassium channel contribute to cardiac repolarization? *J Mol Cell Cardiol* 47: 656–663, 2009. doi:10.1016/j.yjmcc.2009.07.019.
4. **Hamilton S**, **Polina I**, **Terentyeva R**, **Bronk P**, **Kim TY**, **Roder K**, **Clements RT**, **Koren G**, **Choi BR**, **Terentyev D.** PKA phosphorylation underlies functional recruitment of sarcolemmal SK2 channels in ventricular myocytes from hypertrophic hearts. *J Physiol* 598: 2847–2873, 2020. doi:10.1113/JP277618.
5. **Chua SK**, **Chang PC**, **Maruyama M**, **Turker I**, **Shinohara T**, **Shen MJ**, **Chen Z**, **Shen C**, **Rubart-von der Lohe M**, **Lopshire JC**, **Ogawa M**, **Weiss JN**, **Lin SF**, **Ai T**, **Chen PS.** Small-conductance calcium-activated potassium channel and recurrent ventricular fibrillation in failing rabbit ventricles. *Circ Res* 108: 971–979, 2011. doi:10.1161/CIRCRESAHA.110.238386.
6. **Chang PC**, **Hsieh YC**, **Hsueh CH**, **Weiss JN**, **Lin SF**, **Chen PS.** Apamin induces early afterdepolarizations and torsades de pointes ventricular arrhythmia from failing rabbit ventricles exhibiting secondary rises in intracellular calcium. *Heart Rhythm* 10: 1516–1524, 2013. doi:10.1016/j.hrthm.2013.07.003.
7. **Bonilla IM**, **Long VP III**, **Vargas-Pinto P**, **Wright P**, **Belevych A**, **Lou Q**, **Mowrey K**, **Yoo J**, **Binkley PF**, **Fedorov VV**, **Gyorke S**, **Janssen PM**, **Kilic A**, **Mohler PJ**, **Carnes CA.** Calcium-activated potassium current modulates ventricular repolarization in chronic heart failure. *PLoS One* 9: e108824, 2014. doi:10.1371/journal.pone.0108824.
8. **Mizukami K**, **Yokoshiki H**, **Mitsuyama H**, **Watanabe M**, **Tenma T**, **Takada S**, **Tsutsui H.** Small-conductance Ca^{2+}-activated K^+ current is upregulated via the phosphorylation of CaMKII in cardiac hypertrophy from spontaneously hypertensive rats. *Am J Physiol Heart Circ Physiol* 309: H1066–H1074, 2015. doi:10.1152/ajpheart.00825.2014.
9. **Yu CC**, **Corr C**, **Shen C**, **Shelton R**, **Yadava M**, **Rhea IB**, **Straka S**, **Fishbein MC**, **Chen Z**, **Lin SF**, **Lopshire JC**, **Chen PS.** Small conductance calcium-activated potassium current is important in transmural repolarization of failing human ventricles. *Circ Arrhythm Electrophysiol* 8: 667–676, 2015. doi:10.1161/CIRCEP.114.002296.
10. **Nagy N**, **Márton Z**, **Kiss L**, **Varró A**, **Nánási PP**, **Toth A.** Role of Ca^{2+}-sensitive K^+ currents in controlling ventricular repolarization: possible implications for future antiarrhytmic drug therapy. *Curr Med Chem* 18: 3622–3639, 2011. doi:10.2174/092986711796642463.
11. **Jost N**, **Nagy N**, **Corici C**, **Kohajda Z**, **Horvath A**, **Acsai K**, **Biliczki P**, **Levijoki J**, **Pollesello P**, **Koskelainen T**, **Otsomaa L**, **Toth A**, **Papp JG**, **Varro A**, **Virag L.** ORM-10103, a novel specific inhibitor of the Na^+/Ca^{2+} exchanger, decreases early and delayed afterdepolarizations in the canine heart. *Br J Pharmacol* 170: 768–778, 2013. doi:10.1111/bph.12228.
12. **Kohajda Z**, **Farkas-Morvay N**, **Jost N**, **Nagy N**, **Geramipour A**, **Horvath A**, **Varga RS**, **Hornyik T**, **Corici C**, **Acsai K**, **Horvath B**, **Prorok J**, **Ordog B**, **Deri S**, **Toth D**, **Levijoki J**, **Pollesello P**, **Koskelainen T**, **Otsomaa L**, **Toth A**, **Baczko I**, **Lepran I**, **Nanasi PP**, **Papp JG**, **Varro A**, **Virag L.** The effect of a novel highly selective inhibitor of the sodium/calcium exchanger (NCX) on cardiac arrhythmias in in vitro and in vivo experiments. *PLoS One* 11: e0166041, 2016. doi:10.1371/journal.pone.0166041.
13. **Papp R**, **Gonczi M**, **Kovacs M**, **Seprenyi G**, **Vegh A.** Gap junctional uncoupling plays a trigger role in the antiarrhythmic effect of ischaemic preconditioning. *Cardiovasc Res* 74: 396–405, 2007. doi:10.1016/j.cardiores.2007.02.021.
14. **Bers DM**, **Patton CW**, **Nuccitelli R.** A practical guide to the preparation of Ca^{2+} buffers. *Methods Cell Biol* 99: 1–26, 2010. doi:10.1016/B978-0-12-374841-6.00001-3.
15. **Tsuji Y**, **Opthof T**, **Kamiya K**, **Yasui K**, **Liu W**, **Lu Z**, **Kodama I.** Pacing-induced heart failure causes a reduction of delayed rectifier potassium currents along with decreases in calcium and transient outward currents in rabbit ventricle. *Cardiovasc Res* 48: 300–309, 2000. doi:10.1016/s0008-6363(00)00180-2.
16. **Long VP III**, **Bonilla IM**, **Vargas-Pinto P**, **Nishijima Y**, **Sridhar A**, **Li C**, **Mowrey K**, **Wright P**, **Velayutham M**, **Kumar S**, **Lee NY**, **Zweier JL**, **Mohler PJ**, **Gyorke S**, **Carnes CA.** Heart failure duration progressively modulates the arrhythmia substrate through structural and electrical remodeling. *Life Sci* 123: 61–71, 2015. doi:10.1016/j.lfs.2014.12.024.
17. **Pogwizd SM**, **Schlotthauer K**, **Li L**, **Yuan W**, **Bers DM.** Arrhythmogenesis and contractile dysfunction in heart failure: roles of sodium-calcium exchange, inward rectifier potassium current, and residual beta-adrenergic responsiveness. *Circ Res* 88: 1159–1167, 2001. doi:10.1161/hh1101.091193.
18. **Li GR**, **Lau CP**, **Ducharme A**, **Tardif JC**, **Nattel S.** Transmural action potential and ionic current remodeling in ventricles of failing canine hearts. *Am J Physiol Heart Circ Physiol* 283: H1031–H1041, 2002. doi:10.1152/ajpheart.00105.2002.
19. **Li GR**, **Lau CP**, **Leung TK**, **Nattel S.** Ionic current abnormalities associated with prolonged action potentials in cardiomyocytes from diseased human right ventricles. *Heart Rhythm* 1: 460–468, 2004. doi:10.1016/j.hrthm.2004.06.003.
20. **Janse MJ.** Electrophysiological changes in heart failure and their relationship to arrhythmogenesis. *Cardiovasc Res* 61: 208–217, 2004. doi:10.1016/j.cardiores.2003.11.018.
21. **Sah R**, **Ramirez RJ**, **Oudit GY**, **Gidrewicz D**, **Trivieri MG**, **Zobel C**, **Backx PH.** Regulation of cardiac excitation-contraction coupling by action potential repolarization: role of the transient outward potassium current (I_{to}). *J Physiol* 546: 5–18, 2003. doi:10.1113/jphysiol.2002.026468.
22. **Luo CH**, **Rudy Y.** A dynamic model of the cardiac ventricular action potential. II. Afterdepolarizations, triggered activity, and potentiation. *Circ Res* 74: 1097–1113, 1994. doi:10.1161/01.res.74.6.1097.
23. **Akar FG**, **Wu RC**, **Juang GJ**, **Tian Y**, **Burysek M**, **Disilvestre D**, **Xiong W**, **Armoundas AA**, **Tomaselli GF.** Molecular mechanisms underlying K^+ current downregulation in canine tachycardia-induced heart failure. *Am J Physiol Heart Circ Physiol* 288: H2887–H2896, 2005. doi:10.1152/ajpheart.00320.2004.
24. **Rose J**, **Armoundas AA**, **Tian Y**, **DiSilvestre D**, **Burysek M**, **Halperin V**, **O'Rourke B**, **Kass DA**, **Marban E**, **Tomaselli GF.** Molecular correlates of altered expression of potassium currents in failing rabbit myocardium. *Am J Physiol Heart Circ Physiol* 288: H2077–H2087, 2005. doi:10.1152/ajpheart.00526.2003.
25. **Kaab S**, **Dixon J**, **Duc J**, **Ashen D**, **Nabauer M**, **Beuckelmann DJ**, **Steinbeck G**, **McKinnon D**, **Tomaselli GF.** Molecular basis of transient outward potassium current downregulation in human heart failure: a decrease in Kv4.3 mRNA correlates with a reduction in current

density. *Circulation* 98: 1383–1393, 1998. doi:10.1161/01.cir.98.14.1383.

26. **Kaab S**, **Nuss HB**, **Chiamvimonvat N**, **O'Rourke B**, **Pak PH**, **Kass DA**, **Marban E**, **Tomaselli GF.** Ionic mechanism of action potential prolongation in ventricular myocytes from dogs with pacing-induced heart failure. *Circ Res* 78: 262–273, 1996. doi:10.1161/01.res.78.2.262.
27. **Johnson EK**, **Springer SJ**, **Wang W**, **Dranoff EJ**, **Zhang Y**, **Kanter EM**, **Yamada KA**, **Nerbonne JM.** Differential expression and remodeling of transient outward potassium currents in human left ventricles. *Circ Arrhythm Electrophysiol* 11: e005914, 2018. doi:10.1161/CIRCEP.117.005914.
28. **Glukhov AV**, **Fedorov VV**, **Lou Q**, **Ravikumar VK**, **Kalish PW**, **Schuessler RB**, **Moazami N**, **Efimov IR.** Transmural dispersion of repolarization in failing and nonfailing human ventricle. *Circ Res* 106: 981–991, 2010. doi:10.1161/CIRCRESAHA.109.204891.
29. **Chang PC**, **Turker I**, **Lopshire JC**, **Masroor S**, **Nguyen BL**, **Tao W**, **Rubart M**, **Chen PS**, **Chen Z**, **Ai T.** Heterogeneous upregulation of apamin-sensitive potassium currents in failing human ventricles. *J Am Heart Assoc* 2: e004713, 2013. doi:10.1161/JAHA.112.004713.
30. **Jost N**, **Virag L**, **Comtois P**, **Ordog B**, **Szuts V**, **Seprenyi G**, **Bitay M**, **Kohajda Z**, **Koncz I**, **Nagy N**, **Szel T**, **Magyar J**, **Kovacs M**, **Puskas LG**, **Lengyel C**, **Wettwer E**, **Ravens U**, **Nanasi PP**, **Papp JG**, **Varro A**, **Nattel S.** Ionic mechanisms limiting cardiac repolarization reserve in humans compared to dogs. *J Physiol* 591: 4189–4206, 2013. doi:10.1113/jphysiol.2013.261198.
31. **Christophersen P**, **Wulff H.** Pharmacological gating modulation of small- and intermediate-conductance Ca^{2+}-activated K^+ channels (KCa2.x and KCa3.1). *Channels* 9: 336–343, 2015. doi:10.1080/19336950.2015.1071748.
32. **Li W**, **Halling DB**, **Hall AW**, **Aldrich RW.** EF hands at the N-lobe of calmodulin are required for both SK channel gating and stable SK-calmodulin interaction. *J Gen Physiol* 134: 281–293, 2009. doi:10.1085/jgp.200910295.
33. **Adelman JP.** SK channels and calmodulin. *Channels (Austin)* 10: 1–6, 2016. doi:10.1080/19336950.2015.1029688.
34. **Schumacher MA**, **Rivard AF**, **Bachinger HP**, **Adelman JP.** Structure of the gating domain of a Ca^{2+}-activated K^+ channel complexed with Ca^{2+}/calmodulin. *Nature* 410: 1120–1124, 2001. doi:10.1038/35074145.
35. **Joiner WJ**, **Khanna R**, **Schlichter LC**, **Kaczmarek LK.** Calmodulin regulates assembly and trafficking of SK4/IK1 Ca^{2+}-activated K^+ channels. *J Biol Chem* 276: 37980–37985, 2001. doi:10.1074/jbc.M104965200.
36. **Xia XM**, **Fakler B**, **Rivard A**, **Wayman G**, **Johnson-Pais T**, **Keen JE**, **Ishii T**, **Hirschberg B**, **Bond CT**, **Lutsenko S**, **Maylie J**, **Adelman JP.** Mechanism of calcium gating in small-conductance calcium-activated potassium channels. *Nature* 395: 503–507, 1998. doi:10.1038/26758.
37. **Lu L**, **Zhang Q**, **Timofeyev V**, **Zhang Z**, **Young JN**, **Shin HS**, **Knowlton AA**, **Chiamvimonvat N.** Molecular coupling of a Ca^{2+}-activated K^+ channel to L-type Ca^{2+} channels via α-actinin2. *Circ Res* 100: 112–120, 2007. doi:10.1161/01.RES.0000253095.44186.72.
38. **Li N**, **Timofeyev V**, **Tuteja D**, **Xu D**, **Lu L**, **Zhang Q**, **Zhang Z**, **Singapuri A**, **Albert TR**, **Rajagopal AV**, **Bond CT**, **Periasamy M**, **Adelman J**, **Chiamvimonvat N.** Ablation of a Ca^{2+}-activated K^+ channel (SK2 channel) results in action potential prolongation in atrial myocytes and atrial fibrillation. *J Physiol* 587: 1087–1100, 2009. doi:10.1113/jphysiol.2008.167718.
39. **Hsieh YC**, **Chang PC**, **Hsueh CH**, **Lee YS**, **Shen C**, **Weiss JN**, **Chen Z**, **Ai T**, **Lin SF**, **Chen PS.** Apamin-sensitive potassium current modulates action potential duration restitution and arrhythmogenesis of failing rabbit ventricles. *Circ Arrhythm Electrophysiol* 6: 410–418, 2013. doi:10.1161/CIRCEP.111.000152.
40. **Yin D**, **Chen M**, **Yang N**, **Wu AZ**, **Xu D**, **Tsai WC**, **Yuan Y**, **Tian Z**, **Chan YH**, **Shen C**, **Chen Z**, **Lin SF**, **Weiss JN**, **Chen PS**, **Everett T.** Role of apamin-sensitive small conductance calcium-activated potassium currents in long-term cardiac memory in rabbits. *Heart Rhythm* 15: 761–769, 2018. doi:10.1016/j.hrthm.2018.01.016.
41. **Jost N**, **Virag L**, **Bitay M**, **Takacs J**, **Lengyel C**, **Biliczki P**, **Nagy Z**, **Bogats G**, **Lathrop DA**, **Papp JG**, **Varro A.** Restricting excessive cardiac action potential and QT prolongation: a vital role for IKs in human ventricular muscle. *Circulation* 112: 1392–1399, 2005. doi:10.1161/CIRCULATIONAHA.105.550111.
42. **Husti Z**, **Varro A**, **Baczko I.** Arrhythmogenic remodeling in the failing heart. *Cells* 10: 3203, 2021. doi:10.3390/cells10113203.
43. **Hancock JM**, **Weatherall KL**, **Choisy SC**, **James AF**, **Hancox JC**, **Marrion NV.** Selective activation of heteromeric SK channels contributes to action potential repolarization in mouse atrial myocytes. *Heart Rhythm* 12: 1003–1015, 2015. doi:10.1016/j.hrthm.2015.01.027.